Recent changes in the flow of the Ross Ice Shelf, West Antarctica

Christina L. Hulbe [a,*], Ted A. Scambos [b], Choon-Ki Lee [c], Jennifer Bohlander [b], Terry Haran [b]

[a] School of Surveying, University of Otago, PO Box 56, Dunedin, 9054, New Zealand
[b] National Snow and Ice Data Center, University of Colorado, Boulder, CO, USA
[c] Division of Polar Earth System Sciences, Korean Polar Research Institute, Incheon, Republic of Korea

ARTICLE INFO

ABSTRACT

Comparison of surface velocities measured during the Ross Ice Shelf Geophysical and Glaciological Survey (RIGGS, 1973 to 1978) and velocities measured via feature tracking between two Moderate-resolution Imaging Spectroradiometer (MODIS) mosaics (compiled from 2003/4 and 2008/9 images) reveals widespread slowing and minor areas of acceleration in the Ross Ice Shelf (RIS) over the approximately 30 year interval. The largest changes (-13 ma^{-2}) occur near the Whillans and Mercer Ice Streams grounding line in the southernmost part of the ice shelf. Speed has increased over the interval (up to 5 ma^{-2}) between the MacAyeal Ice Stream grounding line and the shelf front, and along the eastern shelf front. Changes in ice thickness computed using ICESat laser altimetry are used together with a well-tested model of the ice shelf to investigate underlying causes of change in the flow of the ice shelf over time. The observed transients represent a combination of recent forcings and ongoing response to ice stream discharge variations over the past millennium. While evidence of older events may be present, the modern signal is dominated by shorter time scale events, including the stagnation of Kamb Ice Stream about 160 years ago, recent changes in basal drag on the Whillans Ice Stream ice plain and, perhaps, iceberg calving. Details in embayment geometry, for example the shallow sea floor below Crary Ice Rise, modulate the spatial pattern of ice shelf response to boundary condition perturbations.

© 2013 Elsevier B.V. All rights reserved.

1. Introduction

The West Antarctic Ice Sheet (WAIS) has the potential for rapid and significant change due to its marine character and fast-flowing ice streams (Alley and Whillans, 1991). Such change is of interest in part because it would affect sea level immediately. The region of the WAIS draining into the Ross Sea was grounded nearly to the edge of the continental shelf at the Last Glacial Maximum, about 20 000 YBP and retreat from that farthest extent appears to have been episodic, not simply directed by an external climate forcing (Conway et al., 1999; Shipp et al., 1999). The prolonged retreat appears to be modulated by the shape of the sea floor and variation in the rate of ice discharge from the interior (Anderson et al., 2002; Hulbe and Fahnestock, 2004, 2007).

Evidence for profound past changes in ice stream discharge is found in many locations in the Ross Sea sector of the WAIS. Buried margin crevasses reveal the stagnation of Kamb Ice Stream to have transpired about 160 years ago, as well as the stagnation of Siple Ice Stream (a distributary of Kamb) 420 ± 60 years ago (Catania et al., 2012; Jacobel et al., 2000; Joughin and Tulaczyk, 2002; Retzlaff and Bentley, 1993). Flow features in the surface of the

Ross Ice Shelf (RIS) have been used to extend the observational record of ice stream discharge variability beyond the instrumental era (Fahnestock et al., 2000). Because the flow of the shelf must adjust to the volume flux of ice discharged into it, physical tracers within the ice form a time-integrated record of past events (MacAyeal et al., 1988). That record indicates that the recent stagnation events are part of a longer term cycle of stagnation and reactivation on century time scales (Hulbe and Fahnestock, 2007). Whillans Ice Stream (WIS) stagnated about 850 years ago and reactivated 400 years later. MacAyeal Ice Stream experienced a similar cycle 800 to 650 years ago.

Whillans Ice Stream (WIS) and the ice plain across which it discharges into the ice shelf is a likely target for change detection because the direct observational record there is relatively long (Bindschadler et al., 2005). The downstream reach of the ice stream (the lightly-grounded ice plain in particular) has been slowing throughout the period of detailed observation, about the last 40 years. Bindschadler et al. (2005) used a careful survey of flow direction, stress regime, and ice thickness time series to conclude that while local (a few ice thicknesses in the horizontal scale) variations were common, there was no clear systematic regional change associated with WIS deceleration, that is, deceleration was neither caused by nor causing detectable changes in ice plain geometry. The most striking changes were in the vicinity of Crary Ice

Rise (Fig. 1)—primarily thinning along its margins—and upstream (thickening) and downstream (thinning) of some ice rumples.

Here we suggest that looking downstream of ongoing changes on grounded ice is the best way to make sense of observations made over time intervals that are short relative to time scales inherent to the system. By examining changing characteristics in the RIS, in particular speed and thickness change, we may be able to determine if the slowdown of WIS is a recent perturbation to a stream that had for some time prior been at steady state or if it is instead part of an ongoing cycle of slow down and speed up. In the latter, then we may be able to infer the processes underlying that cycle. We may also be able to detect changes associated with other outlets, where the direct observational record is more sparse.

Correct interpretation of the ice shelf signal requires consideration of several time scales. Changes in boundary velocity—for example those due to a change in ice stream speed across the grounding line—propagate nearly instantaneously through the ice shelf while changes in ice thickness—those due to changes in ice flux across the grounding line and to changes in ice divergence—propagate on a slower, advective time scale (MacAyeal and Lange, 1988). Changes in the discharge of adjacent ice streams or the location of the grounding line may also be propagated through the coupled momentum and mass balance.

2. Ice velocity

Ice shelves flow by gravity-driven horizontal spreading that transports ice arriving at the grounding line to the calving front. The location of the grounding line is determined by floatation, where the weight of the ice is balanced by buoyancy. Lightly-grounded ice plains at the downstream ends of fast-flowing ice streams broaden the grounding line into a grounding zone. Resistance to ice shelf flow is provided by shear at bay walls, ice rise margins, and the subglacial bed wherever ice runs aground, by compression upstream of ice rises, and by sea water pressure normal to the calving front. At any time, the speed and thickness of the ice depends on the integrated effects of flux across the grounding line, the geometry of the embayment through which the ice flows, mechanical properties of the various materials encountered by the ice, and variations in these over time.

2.1. Velocity measured at the surface

The first spatially comprehensive measurements of Ross Ice Shelf flow speed were made during the Ross Ice Shelf Geophysical and Glaciological Survey (RIGGS) between 1973 and 1978 (Bentley, 1984). The RIGGS program made measurements at nearly 200 stations on the RIS and WIS ice plain, including 72 direct measurements of ice velocity and 77 ice velocities inferred from strain rosette surveys. Those observations mark one time point in the present study (Fig. 1). Errors in the velocity measurements depend on the measurement type and range from less than $5 \, \mathrm{m\,a}^{-1}$ for control stations at camp sites to about $30 \, \mathrm{m\,a}^{-1}$ at the stations interpolated using strain rates. We use the errors reported in appendix Table A1 of Thomas et al. (1984) in our error propagation.

A second epoch of velocities is computed using repeat images of the ice shelf, derived from the MODIS Mosaic of Antarctica mosaic, MOA (Scambos et al., 2007; Haran et al., 2005) spanning late November through February, 2003–2004, and an identically processed mosaic from images acquired in November 2008 through early March 2009 (hereafter, MOA2004 and MOA2009, respectively). The Ross Ice Shelf region is predominantly comprised of images from late December through late January for both mosaics. Image processing details are provided in Scambos et al. (2007), Haran et al. (2005). The range of image acquisition times in each of the two composites (generally 0900 UTC +/− hrs) incorporates
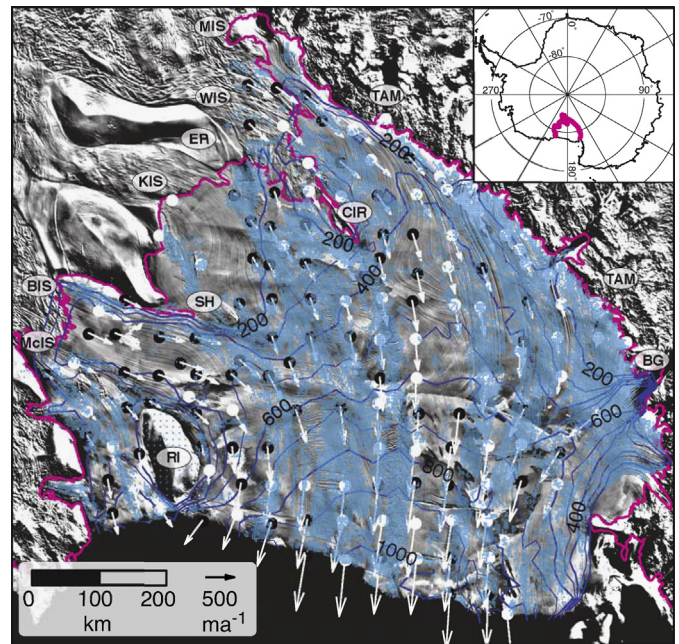
Fig. 1. Ross Ice Shelf with RIGGS and MOA-derived data used in this study. The 1970s RIGGS locations are indicated by black (directly observed) and white (computed using strain rosette measurements) circles with azimuths. The locations of the ∼2006, MOA-derived velocities are shown as blue dots and the speed is contoured at an interval of $100 \, \mathrm{m\,a}^{-1}$. The magenta line here and in other figures is the ice shelf grounding line, the transition across which ice goes afloat. BG: Byrd Glacier; BIS: Bindschadler Ice Stream; CIR: Crary Ice Rise; ER: Engelhardt Ridge; KIS: Kamb Ice Stream; McIS: MacAyeal Ice Stream; MIS: Mercer Ice Stream; RI: Roosevelt Island; SH: Steershead ice rise; TAM: Transantarctic Mountains; WIS: Whillans Ice Stream. (For interpretation of the references to color in this figure legend, the reader is referred to the web version of this article.)

a range of sun azimuths, providing a good image representation of subtle ice shelf features having any orientation. Image stacking and other filtering and data handling methods provide nearly seamless, uniform mosaic images of the snow surface with enhanced surface resolution. Typically 10 to 40 images contributed to each grid cell in the composites over the RIS. Both images are gridded at 125 m scale, and resolution is improved to 150–200 m from the 250 m nominal resolution of the individual MODIS scenes. Some artifacts from surface frost and thin fog remain in the images, but are subdued relative to the enhancement of persistent surface topography by the multi-image stacking approach.

The second velocity field is generated using feature tracking software (Scambos et al., 1992) with the two MODIS mosaic images. Motion is determined by measuring the offset of features, identified and matched by the correlation of small image sub-scenes extracted from the larger images. Several sub-scene sizes are used, ranging from 2 km to 8 km spatial equivalent scale. Small surface features from crevasses, crevasse scars, bottom crevasses, and rift edges move with the ice, and these provide image variations that can be numerically correlated. Errors in the feature tracking depend on pixel size, temporal separation of the two images, and the quality of the correlation matching algorithm. Co-registration errors are estimated at ∼50 m for the geolocation of the individual MODIS scenes (which is likely reduced in the composite MOA2004 and MOA2009 mosaics by averaging of individual scene offsets); feature tracking is accurate to 0.25 to 0.5 pixels (Scambos et al., 1992). The time separation is 5 years. No error is attributed to the compositing period (roughly 35 days for the Ross Ice Shelf section of the two mosaics) because the images are blended into a single surface image representation, and smearing due to motion in the compositing period (typically 50 m, maximum 75 m) would be represented as a sub-grid-cell blurring.
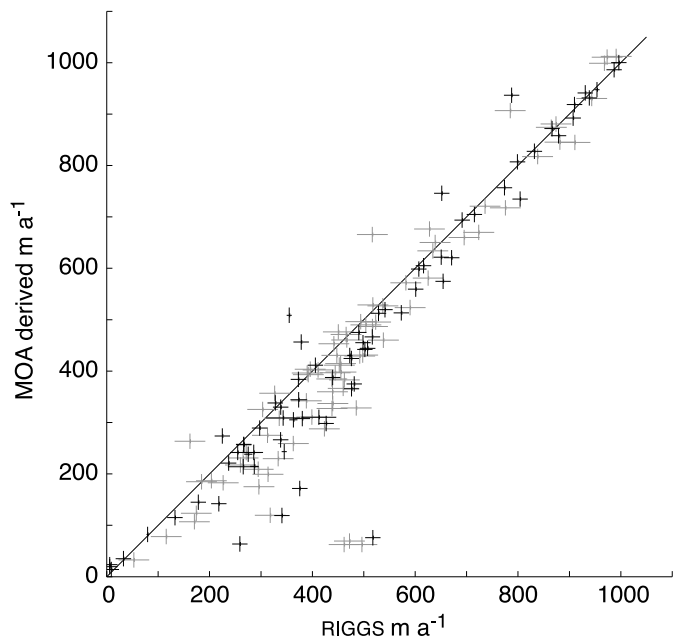
Fig. 2. Comparison between MOA-derived and RIGGS velocities with error bars. Directly observed RIGGS sites are indicated by black while interpolated RIGGS velocities are indicated by gray.

We thus conclude that the error of the MODIS-derived velocity is 15 m a^{-1}, a value that is about 2% of the typical speed measured in the central ice shelf.

2.2. Change over the observation interval

We compare the two data sets in the most straightforward way possible, by finding nearest neighbors to the RIGGS stations in the MOA data set (Fig. 2). In every case we found a neighbor within 4 km of a RIGGS station. Errors are propagated through the difference calculations as the root of the sum of the squares for differences and the root of the sum of the squares divided by the interval length for rates. Only differences that are larger than the error in the difference calculation are discussed here.

Overall, speeds are slower in the recent epoch than they were in the 1970s although ice speed is increasing in some areas (Figs. 2 and 3). The magnitude of the slowing is largest near the WIS and Mercer Ice Stream (MIS) grounding line. Slowing is of course also observed on the WIS ice plain, as has been demonstrated by others (for example Bindschadler et al., 2005; Joughin et al., 2005). Slowing downstream of WIS must be at least in part a response to the ongoing change in flux from the ice stream. This is complicated by Crary Ice Rise (CIR), which is itself a source of change in the region and which obstructs direct communication between the ice stream outlet and the rest of the shelf (Bindschadler et al., 2005; Hulbe and Fahnestock, 2007). Past variation in the discharge of WIS, changes in basal drag on the ice plain, and the recent stagnation of KIS may all influence the transient observed today.

3. Ice thickness

Transients in ice speed are only part of the story of change on the RIS. Because they yield changes to the divergence field, transients in speed should be considered together with transients in the thickness. Here, we use thickness change measured by three-dimensional tracking surface features observed in ICESat (Ice, Cloud, and land Elevation Satellite) laser altimetry (Fig. 4) (Lee et al., 2012) and older observations reported by Bindschadler et
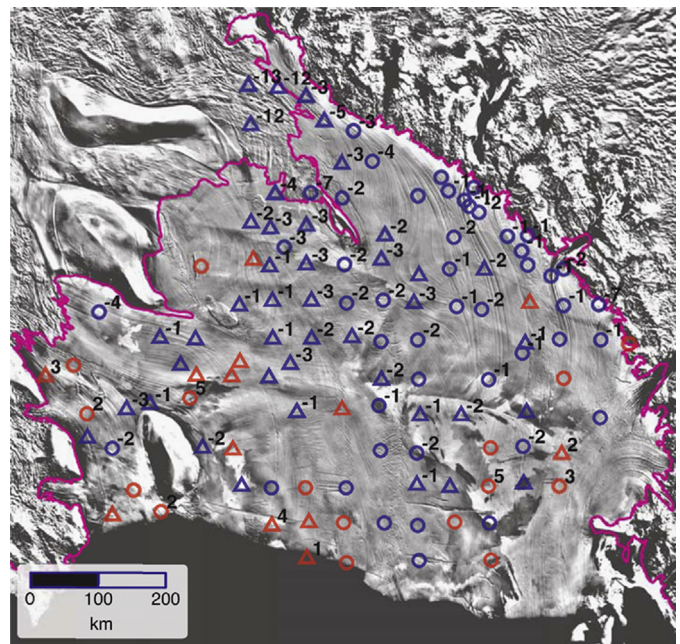
Fig. 3. Linear rate of change over observation interval, approximately 30 years, m a^{-2}. Only values exceeding the propagated error on the rate calculation are displayed. Red symbols indicate an increase and black symbols indicate a decrease. Only in the area of the WIS ice plain does independent information indicate that the rate reported here applies over the entire interval. Circles indicate direct observation in the RIGGS data set while triangles indicate strain rosette data were used. (For interpretation of the references to color in this figure legend, the reader is referred to the web version of this article.)
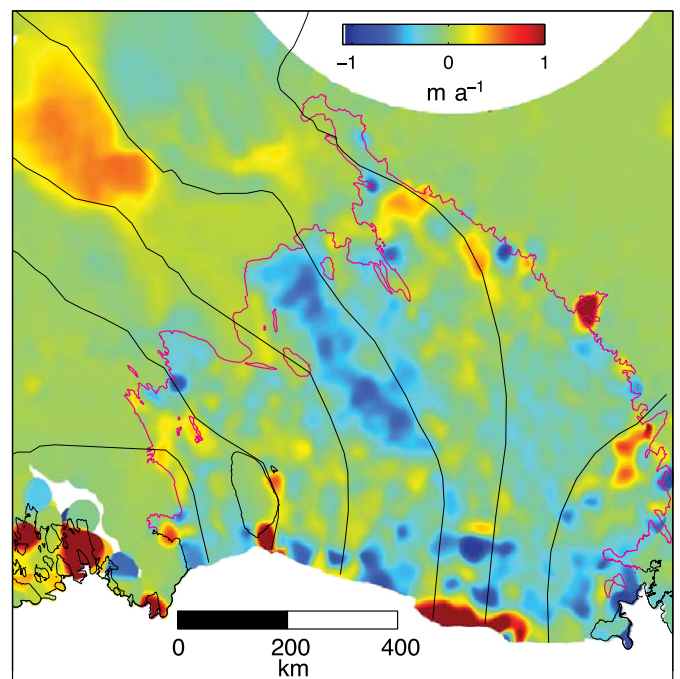
Fig. 4. Linear rate of change in ice thickness from 2003 to 2009 from three-dimensional tracking surface features observed in ICESat laser altimetry. Black lines delineate drainages from the interior to the ice shelf.

al. (2005) (their Fig. 2). Errors in the ICESat-tracking based measurement are approximately 0.04 m a^{-1}. A similar measurement of thickness change is reported in Pritchard et al. (2012).

Thickness change on the floating ice shelf and adjacent ice plains is heterogeneous, reflecting various boundary condition changes and their associated time scales for response across the

whole ice shelf system. It comes as no surprise that ice downstream of the recently stagnated KIS is thinning but this transitions to modest thickening near the shelf front. Ice in the wake of MacAyeal and Bindschadler ice streams is thinning close to the grounding line and thickening farther downstream. Ice in the wake of WIS exhibits a more complicated pattern, thinning immediately upstream of the stagnant ice rise—a perhaps unexpected situation where ice is impinging on a stagnant obstacle (that is, the ice rise)—but thickening over parts of the ice plain further upstream, thickening rapidly between CIR and the Transantarctic Mountains, and thickening modestly downstream of CIR, in the central part of the shelf.

The pattern of thickness change on the WIS and MIS ice plain between 2003 and 2009 appears to be a change relative to an earlier epoch of observation. Bindschadler et al. (2005) compare measurements made around and upstream of Crary Ice Rise at various times between 1958 and 1998 (IGY, RIGGS, and Support Office for Aerogeophysical Research missions) and conclude that most of the ice plain experienced thinning during the earlier intervals. Exceptions are two locations upstream of ice rises, where ice thickened. That is an expected result of ice rise formation, due relative compression upstream of the obstacle. Our interpretation of the changes now underway on the ice plain must account for slowing with thinning over the earlier interval and slowing with thickening more recently.

4. Interpretation

4.1. Model

A numerical ice shelf model that has been used in the past to examine the effect of changing ice stream discharge on ice shelf flow and geometry (Hulbe and Fahnestock, 2007) is used here as a tool to provide context for the new observations. Past volume flux cannot be uniquely determined, but we can test plausible scenarios, using prior work as our guide Catania et al. (2012), Hulbe and Fahnestock (2007).

The most essential components of the model, and special features relevant to this work, are presented here. The model is used to produce transients in ice shelf speed and thickness in response to prescribed changes in ice stream discharge and basal traction on the WIS ice plain. The upstream limit of the model domain is near the present-day grounding line. The transition from grounded to floating may occur anywhere in the domain, depending on flotation. Where ice is grounded, basal traction modifies its flow.

Ice shelf flow is represented by a set of stress-balance equations, simplified by the usual assumption that horizontal flow is depth-independent (MacAyeal and Thomas, 1982). The Glen flow law is embodied in an effective viscosity ν_e that makes use of a depth-average inverse rate factor $\bar{B}$. In a cartesian coordinate system with horizontal coordinates x_i, the stress balance is expressed

$$\frac{\partial}{\partial x_i}\left(2\nu_e h\left(2\frac{\partial u_i}{\partial x_i} + \frac{\partial u_j}{\partial x_j}\right)\right) + \frac{\partial}{\partial x_j}\left(2\nu_e h\left(\frac{\partial u_i}{\partial x_j} + \frac{\partial u_j}{\partial x_i}\right)\right)$$
$$- \rho g h \frac{\partial s}{\partial x_i} - u_i \beta = 0 \qquad (1)$$

where h represents the ice thickness, u represents the horizontal velocity, ρ represents the depth-average density of the ice, g represents the acceleration due to gravity, s represents the surface height, and β is a basal friction parameter that in the case of floating ice is equal to zero and can be set to some non-zero value for ice flowing over an ice plain or rumple (MacAyeal et al., 1995). β is a simple scalar quantity with limited physical meaning beyond its utility in generating basal drag. A no-slip condition is specified at no-flow boundaries such as bay walls, the downstream ends of

interstream ridges, and the edges of stagnant ice rises. The stress-balance equations are solved by iteration on the effective viscosity

$$\nu_e = \frac{\alpha \bar{B}}{2\left[\left(\frac{\partial u_i}{\partial x_i}\right)^2 + \left(\frac{\partial u_j}{\partial x_j}\right)^2 + \frac{1}{4}\left(\frac{\partial u_i}{\partial x_j} + \frac{\partial u_j}{\partial x_i}\right)^2 + \frac{\partial u_i}{\partial x_i}\frac{\partial u_j}{\partial x_j}\right]^{\frac{n-1}{n}}} \qquad (2)$$

in which α is a tuning parameter and the flow-law exponent n is 3.

Following Hulbe and Fahnestock (2007), a spatially variable $\bar{B}$ is generated using an air temperature and the assumption that ice is at the melt temperature at the base. This works well to capture the pattern of speed variation in the interior of the shelf but not near lateral margins. To account for spatially heterogeneous ice properties, we add a spatially variable multiplier α and the product $\alpha\bar{B}$ is tuned by comparison with the RIGGS velocity measurements, as discussed in the cited work.

The ice shelf model infrastructure can correctly reproduce many features of present-day RIS flow, even with a uniform $\bar{B}$ and no notion of basal traction $\beta\mathbf{u}$ on ice plains (MacAyeal et al., 1996). However, modifications to both parameters are necessary to accurately simulate regional details of importance to this study, in particular the pattern of flow around Crary Ice Rise (CIR) (Hulbe and Fahnestock, 2004). The overall rate factor scheme used here was evaluated by Hulbe and Fahnestock (2007) using a chi square test to compare ice speed measured during the RIGGS campaign with modeled ice speed. Special attention is paid to matching the observed flow around CIR in order to avoid unrealistic thickening of ice upstream and adjacent to the ice rise in transient models. A relatively simple spatial variation in α is adequate to this task. Ice moves well through the narrows south of CIR with $\alpha = 0.7$ in a narrow (2 to 3 km) band along the TAM coast from 170 W to 180 W longitude and $\alpha = 0.1$ in a narrow band about 15 km outboard of the southern side of CIR. A narrow band with $\alpha = 0.7$ is applied along the northern margin of CIR. This can be interpreted as softening associated with shear margins in these locations. Other modeling studies, which fail to account for shear margins or the ice plain, or to adequately resolve the narrows between Crary and the TAM, fail to match measured ice speed in this area (MacAyeal et al., 1996).

Basal traction is applied wherever ice runs aground. The parameter β is set at 0.01×10^8 Pa s m^{-1} for model spin-up and through most of the calculations reported here. This value is in line with inversions of surface velocities for basal traction (Sergienko et al., 2008). The corresponding basal drag on the ice plain is small, 0.1 kPa or less. We increase β over time to reproduce changing conditions on the ice plain and the emergence of ice rises. Stagnation is represented by setting the velocity to zero.

Ice shelf thickness varies in response to changing ice stream discharge and basal traction under grounded ice. Mass conservation is expressed

$$\frac{\partial h}{\partial t} = \dot{a} + \dot{b} - \nabla \cdot (\mathbf{u}h) \qquad (3)$$

in which t represents time, $\dot{a}$ and $\dot{b}$ are upper and lower surface accumulation rates and $\mathbf{u}$ represents the vector-valued horizontal velocity. The upper surface ice accumulation rate is specified according to Vaughan et al. (1999). Bottom accumulation, which varies in magnitude and in sign and will certainly change as regions ground and go afloat over time, is not easy to prescribe and is set to zero here.

A model "grounding line" exists wherever adjacent elements in the model mesh have different floatation states. Thus, ice may flow in the stereotypical way, from a grounded element to a floating element, but it may also flow the other way, from floating to grounded. Two conditions are applied at every such boundary, that fluxes and surface slopes match on either side of the

transition. This can result in complicated grounding line geometries where the difference between floating and grounded is only a minor change to the basal stress boundary condition and where slopes on the sea floor are shallow, as is the case at the WIS/MIS and BIS/McIS ice plains (Fig. 1). Our approach captures such geometries.

4.2. Processes and scenarios

Distorted streaklines in the RIS indicate profound past changes in ice stream discharge into the ice shelf. If those changes are part of a longer term cycle related to the ice stream energy budget and subglacial till mechanics (Bougamont et al., 2003; Christoffersen and Tulaczyk, 2003) then it seems likely that ice shelf thickness and flow observed at any particular time do not represent steady state. Time scales associated with different forcings, together with both positive and negative feedbacks, must be accounted for in any interpretation of observed change. For example, declining ice flux applied as an upstream boundary condition would produce an instantaneous effect on the velocity field (Eq. (1)) as well as a longer time scale adjustment as thinner ice advects downstream (Eq. (3)). Thinning due to slowing on an ice plain may cause ice to go afloat, in which case the accompanying reduction in basal traction would cause the ice speed to increase. The speed up relative to grounded ice flow would, in turn, produce new thinning that according to the new basal boundary condition would cause the ice to slow. While they do not simplify the narrative, it is such combinations in time scales and feedbacks that allow transients observed over relatively short time scales to be interpreted in terms of underlying processes.

We wish to examine the observed speed and thickness changes in the context of both recent (the last few decades) and older (centuries ago) events. With this objective in mind, we add a sequence of "*recent*" perturbations to the ice stream discharge and ice rise stagnation chronology identified by Hulbe and Fahnestock (2007) (Table 1 and Fig. 5). Our manipulations are simple and we seek to evaluate their outcomes by comparing patterns of change in the ice speed and thickness throughout the shelf. For the speed transient,

Table 1
Ice stream discharge boundary conditions, and stagnation and reactivation times, used to generate the speed, thickness, and transients shown in Fig. 5. Boundary speeds are in $m\,a^{-1}$, volume fluxes are $km^3\,a^{-1}$, and ages are years before the end of the model run. The KIS outlet narrows prior to stagnation. See Hulbe and Fahnestock (2007) for full details.

Boundary inflow	Speed	Volume	Off	On
Mercer IS	400	7.5		
Whillans IS	550	39	850	450
Kamb IS	500	41	160	
Bindschadler IS	300	13.6		
Siple IS	300	5.0	460	
MacAyeal IS	350	17	800	650
Echelmeyer IS	140	2.2		
Prestrud Inlet	200	1.5		
Scott and Amundsen Glaciers	170	2.7		
Beardmore Glacier	470	4.2		
Nimrod Glacier	250	2.4		
Byrd Glacier	600	11.5		
Mulock Glacier	290	2.1		

we are particularly interested in the largest signal—slowing around CIR that is today larger on the ice plain than in floating ice. The pattern in the thickness transient is more complicated and requires a change in sign on the ice plain—from thickening to thinning directly upstream of CIR and from thinning to thickening throughout most of the rest of the grounded region.

Slowing and thinning on the WIS ice plain implies a decrease in ice flux from farther upstream while slowing and thickening implies an increase in basal traction and perhaps also decreasing flux from upstream. These, then, are the two perturbations we apply in the model. We describe the outcomes of two scenarios here, one in which the only change is declining flux from WIS and the adjacent MIS and one in which both declining flux and increasing β (Eq. (1)) are applied. We associate changing β with changes in the subglacial water and till but do not presume to describe the underlying processes or to specify more than linear rates of change applied uniformly over large regions. The real situation is undoubtedly more complicated than this.

Change near the front of the ice shelf may also be related to iceberg calving. Calving temporarily moves the ice shelf front back
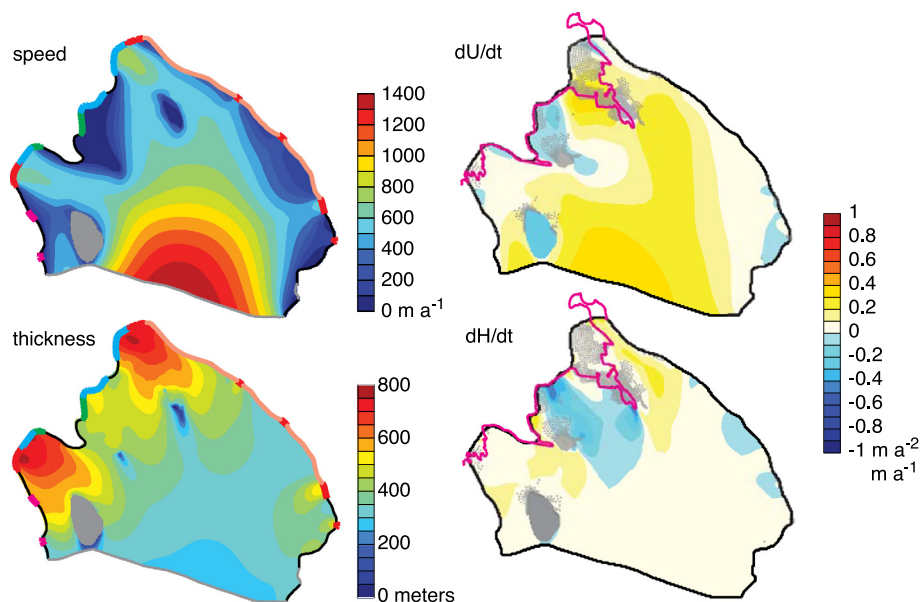
Fig. 5. Model ice speed, thickness, and transients, at the start of the scenarios described in the text. Colored boundaries on the speed and thickness plots indicate influx gates in the model domain. Grey boundaries are shelf front and black boundaries are no-flow. Grey dots indicated nodes in the model domain where ice thickness indicates grounding. The magenta line indicates the location of the observed grounding line.
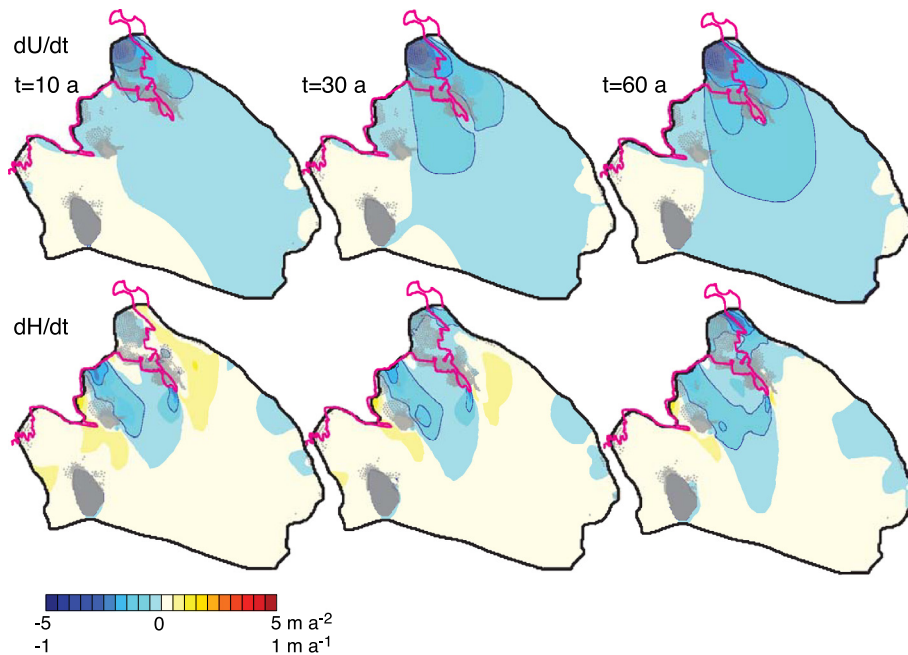
Fig. 6. Rates of change in speed and thickness for a perturbation test in which WIS and MIS flux is decreased. Transients at 10, 30 and 60 years into the test are shown, as labeled. The same color scale is used for all transient plots and the contour intervals are 0.5 m a^{-2} and 0.1 m a^{-1} for the speed and thickness transients, respectively. Grounded ice at the start of the tests described here are as in Fig. 5.

into thicker ice and the perturbation to the stress balance will cause ice near the front to speed up (Scambos et al., 2000). We do not examine this idea any farther here but note that several large calving events took place in the early 2000s.

Ice speed and thickness are both changing at the start of our *recent* scenarios (Fig. 5). Reactivation of WIS 450 years ago following 400 years of quiescence produced an instantaneous speed up and a longer-lived coupled increase in thickness and speed in the wake of the ice stream outlet. Spatial detail in the pattern of these transients depends on the shape of the sea floor—in particular CIR. The stagnation and reactivation of MacAyeal Ice Stream (MacIS) between 800 and 650 years ago also leaves its imprint, in modest positive transients in thickness and speed around Roosevelt Island. Speed at the front of the shelf is increasing as thicker ice associated with WIS and MacIS reactivation continues to advect toward the front. The stagnation of KIS about 150 years ago leaves a wake of thinning 100s of km downstream of the ice stream outlet but only minor slowing. This is because the instantaneous velocity perturbation associated with reduced flux at the ice stream outlet boundary has decayed while the flux-driven thickness transient continues to propagate through the shelf. As was the case for WIS stagnation, propagation of the KIS stagnation effect is modulated by obstacles in the ice flow field—Steershead Ice Rise (SIR) to the north and CIR to the south.

In the following discussion and figures, we use $t = 0$ to indicate the time at which our *recent* boundary condition perturbations are applied. The changes are applied over a 60 year interval (the final 60 years of the complete 1600 year model run). In the first scenario, the flux is decreased approximately 0.2 km^3 a^{-1} per year at the WIS outlet and approximately 0.05 km^3 a^{-1} per year at MIS outlet. These correspond to speed changes of 2.5 m a^{-1} per year. In the second scenario, β rises linearly on the ice plain, from a value of 0.1×10^8 to 1×10^8 Pa m s^{-1}, except in a narrow region between the downstream tip of CIR and Engelhardt Ridge, where β remains unchanged. Leaving this region unchanged reduces the magnitude of slowing through that relatively narrow gate.

4.3. Ice speed

The WIS and MIS flux reduction is applied as linear change in a flux boundary condition, generating both instantaneous kinematic effects and longer time scale advective effects (Fig. 6). Thus while the effect is always larger closer to the site of the perturbation over the 60 model years, the area affected by the perturbation increases as the change persists. Details in the pattern of change depend on the shape of the sea floor and the traction applied to the base of the ice where it is run aground. If CIR was not stagnant, the flux perturbation would more readily propagate into the interior of the shelf.

Increasing basal traction on the ice plain yields a different pattern in the speed transient (Fig. 7), in part because it moves the perturbation away from the model boundary and closer to CIR. This allows the speed change to more easily propagate past the ice rise than in the first scenario. The effect, however, is short lived. As modeled ice speed adjusts to the changed traction parameter, the pattern of change in the ice speed change pattern returns to the flux-perturbation pattern (compare $t = 60$ in Figs. 6 and 7). Changing the magnitude of the β perturbation would change the magnitude of the response in u but not the pattern. A more complicated manipulation of β could, of course, change the pattern but we are not prepared to speculate in that regard. We do note that the largest basal drag produced by our change to β is about 1.7 kPa, about half the magnitude of a value deduced by Walter et al. (2011). Larger β would produce an even better match. The peak change in ice speed is about -13 m a^{-2} (not at the same time as the peak basal drag, see Fig. 8).

4.4. Ice thickness

Ice shelf thickness may change for mechanical or thermal reasons (melting, firn densification). Firn processes were addressed in the thickness change calculation (Lee et al., 2012) and our interest here are changes associated with ice mechanics. Thus, we emphasize the pattern of relative change through the ice shelf.
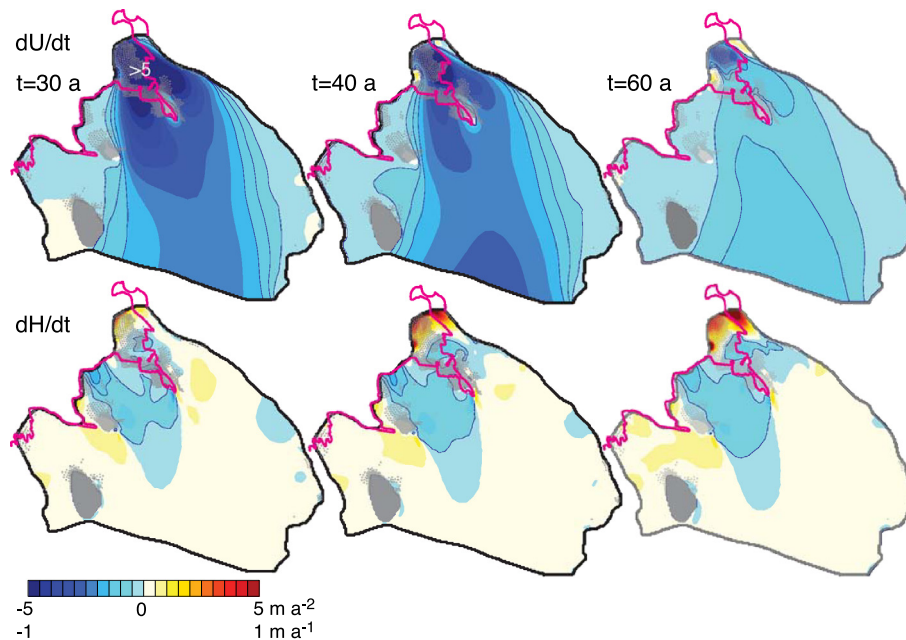
Fig. 7. Rates of change as in Fig. 6 for a test in which WIS and MIS flux is decreased and the basal traction parameter is increased for grounded ice downstream of those ice streams. The transient at 10 years is as in Fig. 6 so rates at 30, 40, and 60 years are shown for this test. The large initial response to a change in basal traction decays rapidly for ice speed and persists for ice thickness.
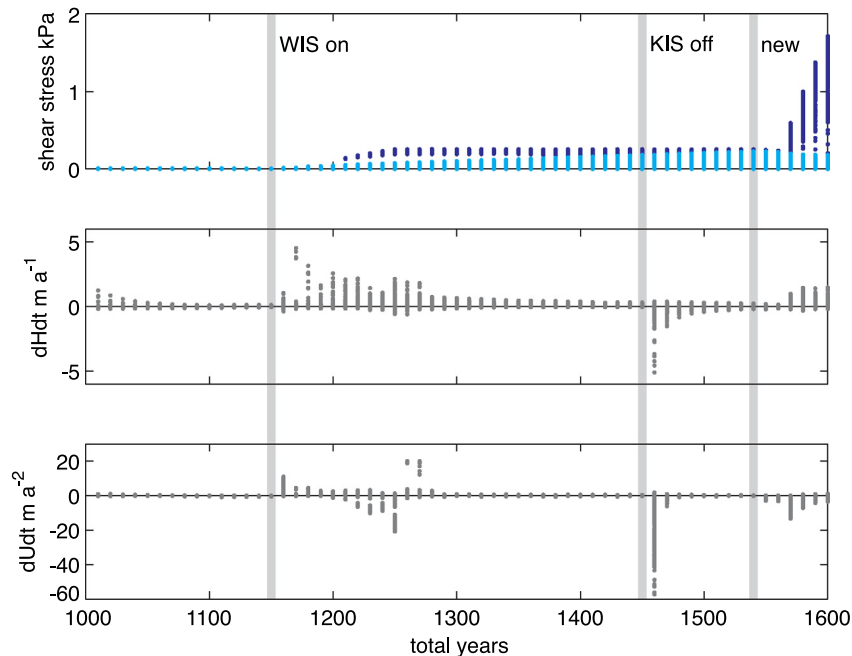
Fig. 8. Basal drag and rates of change for model nodes grounded on the WIS and MIS ice plain over time in the second experiment. The plot starts at 600 years before the end of the model run, a time when MacAyeal Ice Stream has just reactivated after an episode of stagnation. The basal traction parameter β increases from 0.01×10^8 to 0.1×10^8 Pa m s^{-1} from 1150 to 1050 and then to 1×10^8 Pa m s^{-1} from 1540 to the end of the model run. The resulting effect on basal drag is shown in the top panel, with dark blue representing most of the ice plain and light blue representing the narrow strip between the upstream end of CIR and the downstream end of Englehardt Ridge, where β remained set at 0.1×10^8 Pa m s^{-1}. The complete sequence of boundary condition changes are reviewed in Table 1. The final 60 years comprise the experiments reported in the text. (For interpretation of the references to color in this figure legend, the reader is referred to the web version of this article.)

Ice-mechanical effects may be accompanied by changes in basal melting, which we do not attempt to include.

At $t = 0$, ice thickness is changing in response to both the relatively distant reactivation of WIS and the recent stagnation of KIS. The shallow sea floor and stagnation of ice at Crary and Steershead ice rises confines the region of thinning associated with KIS stagnation, while modest thickening in response to WIS and MacIS reactivation centuries ago continues in the model. Thick-

ening is ongoing upstream of CIR, where ice must flow around the obstacle. CIR also poses a barrier to propagation of the thickness change when a new epoch of WIS deceleration is added to the model (Fig. 6). Details in the pattern reflect the contrast between the flow of grounded and floating ice. Where ice is floating south of CIR, the rate of thickness change is relatively rapid, while grounded ice responds more slowly to the same perturbation. The region of thickening—remnant from the last cycle of WIS

discharge variability—is gradually overprinted by the new perturbation. The pattern of thinning upstream and (residual) thickening downstream in the floating ice at $t = 30$ may be similar to that in the ICESat-derived measurement (Fig. 4), although another interpretation is also possible.

The response of the model thickness field to simultaneous changes in WIS flux and β (Fig. 7) is more spatially variable than in the flux-change only case. Both thinning and thickening occur on the WIS and MIS ice plain, even though the modification to β is uniform. When basal drag (βu) increases, the overlying ice responds by slowing and thickening. The magnitude of the change is larger closer to the source of new ice—the flux gate in the model. This reduces flux to locations farther downstream, producing a pattern of thickening and thinning between the flux gate and CIR much like the observed 2003 to 2009 transient. The pattern in the observed transient, interpreted using the ice shelf model, implies a recent change in basal traction on the ice plain (recall that the older pattern was opposite to this pattern). Where thickening ice spreads across the grounding line, floating ice in the narrows between CIR and the TAMs also thickens. Thus, the observed thickening south of CIR (Fig. 4) could be interpreted as a response to changing basal drag on the ice plain, not only as a remnant of long past events. Again, CIR and SIR act to constrain the region over which these perturbations are propagated.

5. Conclusion

Transients measured in the Ross Ice Shelf today represent an integrated history of change to its boundary conditions. Because driving stresses are not locally balanced on the floating ice, changes in boundary conditions anywhere produce instantaneous adjustments to ice velocity everywhere. Corresponding changes in mass flux propagate the perturbation forward in time as adjustments to ice thickness. Where thickness changes cause ice to run aground or go afloat, additional perturbations to boundary conditions result. Ongoing changes to boundary conditions, for example declining flux from an ice stream, produce ongoing instantaneous and advective adjustments to the velocity and thickness of the ice. The passage of time, the types, and magnitudes of past events all govern the magnitude and pattern with which past events are expressed, and thus our ability to attribute what we measure to particular forcings. Seen in a more positive light, those patterns in space and time offer an opportunity to infer past events.

The outlet of WIS has been slowing over at least the last four decades. This ongoing perturbation to a boundary flux must thus be in part responsible for deceleration, where it is observed, on the ice shelf (Fig. 3). The observed ice shelf thickness change (Fig. 4) complicates interpretation of the speed change because it requires slowing to be accompanied in some locations by thickening. Thickening requires us to add another process to our interpretation. With regard to the history WIS discharge, we do not know if the flux was declining prior the earliest (1970s) measurements but the positive thickness transients distant from the ice stream outlet suggest that it was not.

Older changes in ice stream flux account for thickness transients in some locations—thickening around Roosevelt Island in response to the reactivation of MacIS and thinning downstream of KIS in response to its stagnation. The instantaneous effects associated with those ice stream flux changes have decayed away (Fig. 8) but advective effects may be still be in action. Coupled thickness and speed transients associated with these older events have relatively small magnitudes today but may be expressed far from the source of the original boundary condition perturbation (that is, far from the grounding line).

The relatively large magnitudes of the speed changes calculated here require recent changes to boundary conditions. The nature of those changes, however, cannot be inferred from the speed change measurement on its own—both declining flux and increasing basal traction can produce transients in the ice speed that mimic the observations. An additional measurement—change in ice thickness—is required to identify the correct forcing (or combination of forcings). In the case of the WIS and MIS ice plain, we conclude that both declining flux and increasing basal traction are required and that the declining flux from upstream appears to have preceded the change to the basal boundary condition on the ice plain. It is possible that earlier changes in basal conditions affected the ice flux but we do not have data that might be used to investigate such a possibility.

The observed increases in speed and thickening in the eastern region of the RIS may in part be an ongoing response to reactivation of MacIS 650 years before the end of the model time series. The patterns and magnitudes match reasonably well with transients prior to our recent WIS and MIS manipulations (Fig. 5). Those patterns are preserved in the WIS and MIS flux-change only case but the speed transient is overprinted in the flux and basal traction change case. This may indicate that we have underestimated one perturbation and overestimated the other or it may indicate a missing process. One such process is iceberg calving. The calving of iceberg B-15 in the year 2000 would have caused a transient speed up around and upstream of Roosevelt Island as the shelf front retreated into relatively thicker ice.

The implications regarding variation in conditions at the ice/bed interface are interesting. Our models produce better outcomes when basal traction is spatially heterogeneous (here we make the bed between CIR and Englehardt Ridge less still than elsewhere on the WIS and MIS ice plain). We cannot determine the timing or detailed spatial pattern with which changes in traction transpire but our analysis is in line with the conclusion drawn by Bindschadler et al. (2005), that the ongoing slowdown was not driven by a mass imbalance and must instead involve changes at the bed.

References

Alley, R.B., Whillans, I.M., 1991. Changes in the West Antarctic ice sheet. Science 254, 959–963.

Anderson, J., Shipp, S., Lowe, A., Wellner, J., Mosola, A., 2002. The Antarctic ice sheet during the last glacial maximum and its subsequent retreat history: A review. Quat. Sci. Rev. 21, 49–70.

Bentley, C., 1984. The Ross Ice Shelf geophysical and glaciological survey (RIGGS): Introduction and summary of measurements performed. In: Hayes, D., Bentley, C. (Eds.), Antarct. Res. Ser., vol. 42. American Geophysical Union, Washington, DC, pp. 1–20.

Bindschadler, R., Vornberger, P., Gray, L., 2005. Changes in the ice plain of Whillans Ice Stream, West Antarctica. J. Glaciol. 51, 620–636.

Bougamont, M., Tulaczyk, S., Joughin, I., 2003. Numerical investigations of the slowdown of Whillans Ice Stream, West Antarctica: Is it shutting down like ice stream c? Ann. Glaciol. 37, 239–246.

Catania, G.A., Hulbe, C.L., Conway, H., Scambos, T.A., Raymond, C.F., 2012. Variability in the mass flux of the Ross ice streams, West Antarctica, over the last millennium. J. Glaciol. 58. 12 pp., http://dx.doi.org/10.3189/2012JoG11J219.

Christoffersen, P., Tulaczyk, S., 2003. Thermodynamics of basal freeze-on: Predicting basal and subglacial signatures of stopped ice streams and interstream ridges. Ann. Glaciol. 36, 233–243.

Conway, H., Hall, B.L., Denton, G.H., Gades, A.M., Waddington, E.D., 1999. Past and future grounding-line retreat of the West Antarctic ice sheet. Science 286, 280–283.

Fahnestock, M., Scambos, T., Bindschadler, R., Kvaran, G., 2000. A millennium of variable ice flow recorded by the Ross Ice Shelf, Antarctica. J. Glaciol. 46, 652–664.

Haran, T., Bohlander, J., Scambos, T., Fahnestock, M., 2005. MODIS mosaic of Antarctica (MOA) image map. Digital media. National Snow and Ice Data Center, Boulder, CO, USA.

Hulbe, C.L., Fahnestock, M.A., 2004. West Antarctic ice stream discharge variability: Mechanism, controls, and pattern of grounding line retreat. J. Glaciol. 50, 471–484.

Hulbe, C., Fahnestock, M., 2007. Century-scale discharge stagnation and reactivation of the Ross ice streams, West Antarctica. J. Geophys. Res. 112.

Jacobel, R., Scambos, T., Nereson, N., Raymond, C., 2000. Changes in the margin of ice stream C, Antarctica. J. Glaciol. 46, 102–110.

Joughin, I., Tulaczyk, S., 2002. Positive mass balance of Ross ice streams, West Antarctica. Science 295, 476–480.

Joughin, I., Bindschadler, R., King, M., Voight, D., Alley, R., Anandakrishnan, S., Horgan, H., Peters, L., Winberry, P., Das, S., Catania, G., 2005. Continued deceleration of Whillans Ice Stream, West Antarctica. Geophys. Res. Lett. 32. 4 pp.

Lee, C.K., Seo, K.W., Han, S.H., Yu, J., Scambos, T.A., 2012. Ice velocity estimation in the Ross Ice Shelf by matching surface undulations measured by ICESat laser altimetry. Remote Sens. Environ. 124, 251–258.

MacAyeal, D.R., Lange, M.A., 1988. Ice-shelf response to ice-stream discharge fluctuations: II. Ideal rectangular ice shelf. J. Glaciol. 36 (116), 128–135.

MacAyeal, D.R., Thomas, R.H., 1982. Numerical modeling of ice shelf motion. Ann. Glaciol. 3, 189–193.

MacAyeal, D.R., Bindschadler, R.A., Jezek, K.C., Shabtaie, S., 1988. Can relict crevasse plumes on Antarctic ice shelves reveal a history of ice-stream fluctuation? Ann. Glaciol. 11, 77–82.

MacAyeal, D.R., Bindschadler, R.A., Scambos, T.A., 1995. Basal friction of ice stream E, West Antarctica. J. Glaciol. 41 (138), 247–262.

MacAyeal, D.R., Rommelaere, V., Huybrechts, P., Hulbe, C.L., Determann, J., Ritz, C., 1996. An ice-shelf model test based on the Ross Ice Shelf, Antarctica. Ann. Glaciol. 23, 46–51.

Pritchard, H., Ligtenberg, S., Fricker, H., Vaughan, D., van den Broeke, M., Padman, L., 2012. Antarctic ice-sheet loss driven by basal melting of ice shelves. Nature 484, 502–505.

Retzlaff, R., Bentley, C.R., 1993. Timing of stagnation of ice stream C, West Antarctica from short-pulse radar studies of buried surface crevasses. J. Glaciol. 39, 553–561.

Scambos, T., Dukiewicz, M., Wilson, J., Bindschadler, R., 1992. Application of image cross-correlation to the measurement of glacier velocity using satellite image data. Remote Sens. Environ. 42, 177–186.

Scambos, T., Hulbe, C., Fahnestock, M., Bohlander, J., 2000. The link between climate warming and break-up of ice shelves in the Antarctic Peninsula. J. Glaciol. 46, 516–530.

Scambos, T., Haran, T.M., Fahnestock, M.A., Painter, T.H., Bohlander, J., 2007. MODIS-based Mosaic of Antarctica (MOA) data sets: Continent-wide surface morphology and snow grain size. Remote Sens. Environ. 111.

Sergienko, O.V., Bindschadler, R.A., Vornberger, P.L., MacAyeal, D.R., 2008. Ice stream basal conditions from block-wise surface data inversion and simple regression models of ice stream flow: Application to Bindschadler Ice Stream. J. Geophys. Res. 113. 11 pp.

Shipp, S., Anderson, J.B., Domack, E.W., 1999. Late Pleistocene–Holocene retreat of the West Antarctic Ice-Sheet system in the Ross Sea: Part 1, Geophysical results. Geol. Soc. Am. Bull. 111, 1486–1516.

Thomas, R.H., MacAyeal, D.R., Eilers, D.H., Gaylord, D.R., 1984. Glaciological studies on the Ross Ice Shelf, Antarctica: 1973–1978. In: Antarct. Res. Ser., vol. 42, pp. 21–53.

Vaughan, D.G., Bamber, J.L., Giovinetto, M.B., Russell, J., Cooper, A.P.R., 1999. Reassessment of net surface mass balance in Antarctica. J. Climate 12, 933–946.

Walter, J., Brodsky, E., Tulaczyk, S., Schwartz, S.Y., Pettersson, R., 2011. Transient slip events from near-field seismic and geodetic data on a glacier fault, Whillans ice plain, West Antarctica. J. Geophys. Res. 116. 13 pp.